



How the forcing dynamics of the western boundary currents in the Pacific respond to the North Equatorial Current

Junlu Li^{a,b}, Jianping Gan^{a,b,*}

^a Center for Ocean Research in Hong Kong and Macau, Department of Ocean Science and Department of Mathematics, The Hong Kong University of Science and Technology, China

^b Earth, Ocean and Atmospheric Sciences, The Hong Kong University of Science and Technology (Guangzhou), Guangzhou, China

ARTICLE INFO

Keywords:

Western North Pacific
Western boundary currents
Vorticity dynamics
Seasonality
Numerical model

ABSTRACT

Applying a layer-integrated vorticity balance to the North Equatorial Current (NEC)-Kuroshio Current (KC)-Mindanao Current (MC) system, we found that the intensities of the circulations composed by NEC-KC and NEC-MC in the corresponding northern and southern NEC-KC-MC (NKM) sub-domains control the KC and MC, respectively. The planetary vorticity fluxes associated with the NEC, KC, and MC volume transports externally dominates the inter-linked NKM circulations, and the prominent nonlinearities with the western boundary currents internally determine the dynamic response. The net planetary vorticity loss in the northward KC and vorticity gain in the westward NEC dominate the vorticity budget in their respective sub-domains and subsequently lead to a corresponding relative vorticity convergence and divergence in the downstream-accelerating KC and MC. Impacts of the negative/positive vorticity from wind stress curl (WSC) accelerate/decelerate the KC, while the positive vorticity impart from the WSC accelerates the MC throughout the year. Bottom pressure torque produced by tilting isopycnals contributes an amount comparable to what the WSC contributes to the circulation in the western boundary region. This study reveals the connection between the KC/MC and the corresponding regional circulations and advances our understanding of the underlying mechanisms in the NKM system and quantifies the interacting external/intrinsic physical inter-connection. This dynamic study is a companion to Li and Gan's (2022) kinematic study where they investigated what the NKM modes of three physical features: intensity, migration, and bifurcation location contribute to the transports of the KC and the MC.

1. Introduction

The basin-scale North Equatorial Current (NEC, see Table 1 for abbreviations used in this manuscript) bifurcates into the northward Kuroshio Current (KC) and southward Mindanao Current (MC) at the east coast of the Philippines in the western Pacific Ocean (WPO, Fig. 1). These three currents in the upper ocean form the NEC-KC-MC (NKM) circulation system, which is significant to the transport of water, heat, and energy in the North Pacific, and has further impact on climate change (Gan et al. 2016a; Hu et al. 2015; Nan et al. 2015).

The KC and MC are strong and narrow western boundary currents (WBCs) in the WPO, carrying the tropical NEC water meridionally to mid-latitude and equatorial regions, respectively (Hu et al. 2015; Kashino et al. 2005; Kashino et al. 2009; Qu et al. 1998a; Ren et al. 2018). These two WBCs vary seasonally with the NKM circulation

system to affect the regions downstream. The KC flows past Luzon Island and enters the South China Sea through Luzon Strait, generating water and energy exchange between the WPO and the South China Sea (Centurioni et al. 2004; Farris and Wimbush 1996; Tian et al. 2006). The main stream of the KC flows back into the WPO and intensifies along the east coast of Taiwan and the continental slope of the East China Sea (Chen et al. 1995; Liu and Gan 2012), which finally forms the Kuroshio Extension southeast of Japan. The MC flows into the equatorial region and joins the eastward North Equatorial Countercurrent with partly feeding into the Indonesia Throughflow across the Celebes Sea (Gordon 1986).

Previous studies characterized the general pattern of the circulation and the variability of the NKM. The NEC of ~ 50 Sv is distributed into the KC and MC with comparable volume transports (Gan et al. 2016b; Kashino et al. 2009; Nitani 1972; Qiu and Lukas 1996; Qu et al. 1998a;

* Corresponding author.

E-mail address: magan@ust.hk (J. Gan).

Table 1
List of abbreviations.

Abbreviation	Definition
NEC	North Equatorial Current
KC	Kuroshio Current
MC	Mindanao Current
NKM	NEC-KC-MC
WSC	Wind Stress Curl
WPO	Western Pacific Ocean
WBC	Western Boundary Current
CMOMS	China Sea Multiscale Ocean Modeling System
INT	Transport by NEC Intensity effect
MIG	Transport by NEC Migration effect
BIF	Transport by NEC Bifurcation location effect
NB	NEC Bifurcation
CC	Correlation Coefficient
LIVE	Layer-Integrated Vorticity Equation
PGF	Pressure Gradient Force
ACC	Acceleration
NPV	Net Planetary Vorticity
NL	Nonlinearity
HVISC	Horizontal Viscosity
VADV	Vertical Advection
BPT	Bottom Pressure Torque
NSC	Net Stress Curl

Toole et al. 1988; Wang et al. 2015). Vertically, the three upper layer currents (i.e., the NEC, KC, and MC) change their direction below ~ 500 m, where the Luzon Undercurrent, Mindanao Undercurrent, and North Equatorial Undercurrent form the subsurface circulation system in the middle layer (~500 to 2000 m) (Hu and Cui 1989; Hu et al. 1991; Hu et al. 2013; Li and Gan 2020; Qiu et al. 2013; Qu et al. 1998b; Wang et al. 2015). Three aspects of the NEC contribute to the seasonal variation of

the KC and MC transports: the NEC intensity, migration, and bifurcation location (Li and Gan 2022). Li and Gan (2022) isolated and quantified the contributions of these three aspects with distinct physical meanings and concluded that the NEC intensity, while being modulated by the offsetting NEC migration and bifurcation location, dominates the variability of the KC and MC (Fig. 1).

Past researchers used observations and model simulations to widely study the dominant features and characteristics of the NKM circulation. However, we still do not fully understand the dynamics and underlying mechanisms of the spatiotemporal variability of the WBCs. Qu et al. (2012) used momentum equation to separate the geostrophic and ageostrophic velocity in the MC and Mindanao Undercurrent. The geostrophic portion is claimed to be supported by pressure gradient due to the water accumulation towards the shore (Qu et al. 2012). Wang et al. (2015) also pointed out that pressure gradient generated by sea level gradient is responsible for the upper layer currents, including the NEC, KC and MC. The previous dynamic investigations of the NKM circulation system were lack of evidence for the formation of the dominant forcing, i.e. the pressure gradient force. In addition, the different physical processes and controlling mechanisms were not quantitatively calculated. The existing fragmented dynamic studies cannot provide the systematic mechanism driving the holistic NKM circulation because of limited observations and insufficient theory. To fill the gap in the dynamic understanding of the variable KC and MC and corresponding quantitative investigation, we utilized simulations from the validated China Sea Multiscale Ocean Modeling System (CMOMS) to conduct process-oriented analyses of the WBCs and the associated NKM circulation system in the WPO.

We based this dynamic study on the kinematic investigation presented by Li and Gan (2022) in which they found the spatiotemporal

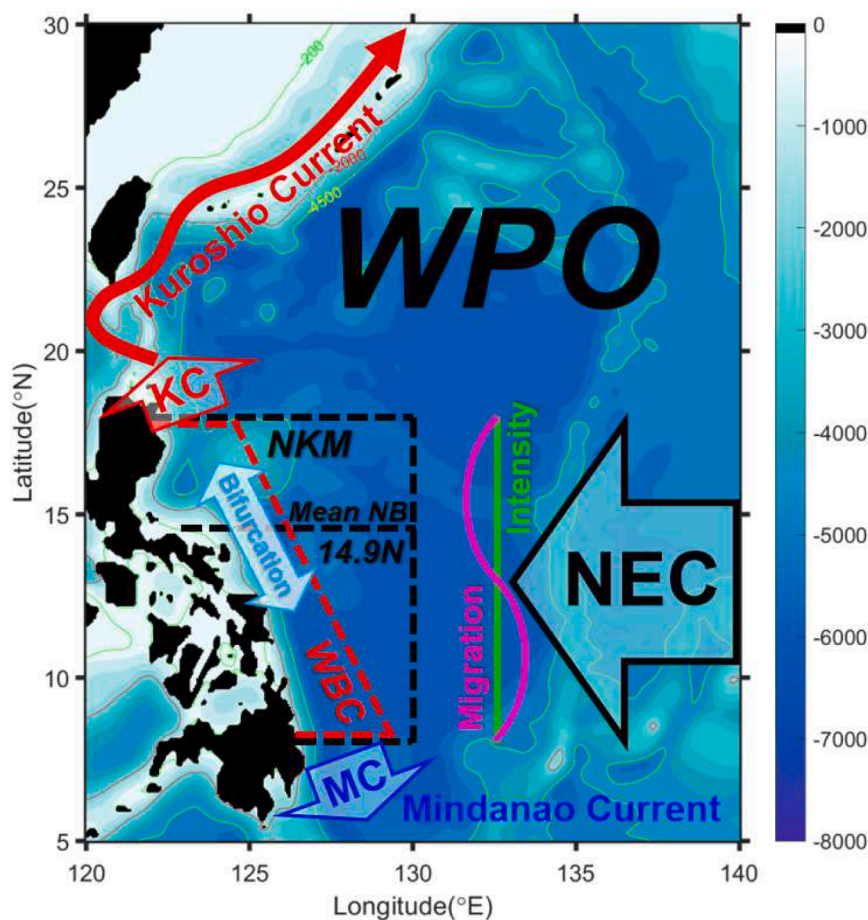


Fig. 1. Bathymetry (m) and schematic of the upper layer circulation in the Western Pacific Ocean (WPO). The North Equatorial Current (NEC), Kuroshio Current (KC), and Mindanao Current (MC) link at the NEC Bifurcation (NB). The box surrounded by the black dashed line indicates the NEC-KC-MC (NKM) domain. The WBC domain is bounded by the dashed red line, and they are both separated by the annual mean NB at 14.9°N into the northern and southern sub-domains. The three NEC characteristics investigated by Li and Gan (2022) are illustrated by the green line, magenta line, and cyan arrows, respectively.

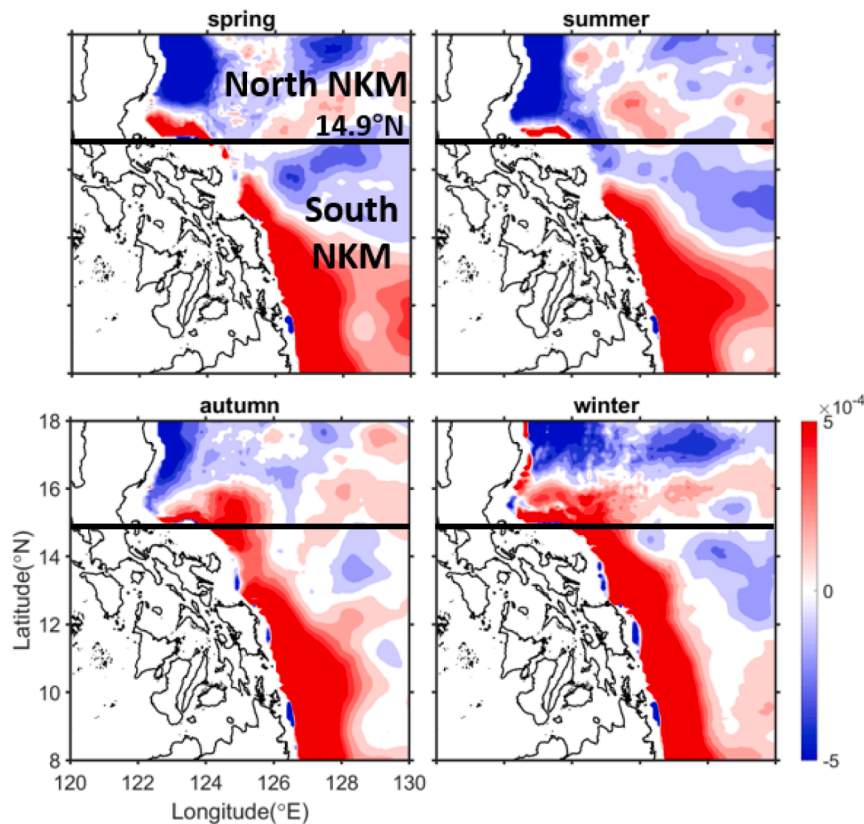


Fig. 2. The seasonally mean relative vorticity (m s^{-1}) of the layer-integrated volume flux in (a) spring, (b) summer, (c) autumn, and (d) winter. The annual mean NB at latitude 14.9°N divides the NKM domain into the northern (North NKM) and southern (South NKM) sub-domains.

modes determined by three physical aspects linked the NEC with the WBCs. The objective of our study is to reveal the underlying dynamics of the features and connections within the NKM circulation. To this end, we first reveal the physical connection between the intensities of the WBCs and the circulations in the NKM sub-domains based on Stokes' theorem. With vorticity dynamics, we then link the external forcing of the planetary vorticity fluxes to the intrinsic dynamic responses produced by nonlinearity, bottom pressure torque, and wind stress curl. The three NEC characteristics of intensity, migration, and bifurcation location that Li and Gan identified describe the volume transports across the boundaries of the enclosed sub-domains, and these three characteristics directly depict the planetary vorticity carried by the currents. This study elevates our knowledge of the holistic NKM circulation and KC/MC, including the physical inter-connections and forcing dynamics. The dynamic approaches and new understanding will be useful to studies of other WBCs in the global oceans.

2. Description of the Ocean model

The CMOMS (Gan et al. 2016a; Gan et al. 2016b) is based on the Regional Ocean Model System (Shchepetkin and McWilliams 2005). Following Li and Gan (2022), we used CMOMS to conduct a dynamic study of the NKM circulation and WBCs in the WPO. For the vertical mixing parameterization, we adopted a local closure scheme based on the level-2.5 turbulent kinetic energy equations (Mellor and Yamada 1982). The model domain covered the China Seas, the Japan Sea, and part of the WPO, which was sufficient for focusing on the NKM region. We merged ETOPO5 data from the National Geophysical Data Center, and digitized water depths, extracted from the navigation maps published by the China Maritime Safety Administration, to provide the topography and coastline. The horizontal resolution was $\sim 0.1^\circ$ which resolved the meso-scale processes. Vertically, we adopted 30-layer

stretched terrain-following coordinates with higher resolution at the surface and bottom boundary layers.

We forced the model with the daily wind stress derived from the blended 0.25° sea surface winds released by the National Oceanic and Atmospheric Administration and the National Climatic Data Center (<https://www.ncei.noaa.gov/products/blended-sea-winds>), and daily heat/freshwater fluxes adopted from reanalysis meteorological data released by the National Centers for Environmental Prediction based on bulk formulation (Fairall et al. 2003). We integrated the open boundary conditions (OBCs) along the eastern and southern open boundaries of the model domain with active OBCs (Gan and Allen 2005) and Tidal-Subtidal (TST) OBCs (Liu and Gan 2016), which concurrently accommodate tidal and subtidal forcing. The sea surface elevation, three-dimensional velocities, temperature, and salinity along the open boundaries were from the Ocean General Circulation Model for the Earth Simulator (OFES) (Sasaki et al. 2008).

We spun up the model with climatological monthly forcing and lateral fluxes for 50 years to produce the climatology simulation. The variables averaged in winter (November, December, and January) over the last 5 years of the climatology simulation provided the initial conditions for the direct simulation. We applied lateral fluxes provided by OFES from 1988 to 2012 as the boundary condition. To avoid unstable fluctuations in the first few years, we only used the results from 1993 to 2012 to calculate the climatological annual cycle for this study. Detailed configuration and validation of the model were published in the following studies: (Gan et al. 2016a; Gan et al. 2016b; Liu and Gan 2017).

3. Characteristics and dynamics of the NKM circulation

3.1. General circulation

The NKM circulation in the upper-layer WPO is important to the

distribution of water and energy in the North Pacific. Li and Gan (2022) summarized the characteristics of the NKM circulation. The NEC velocity core at $\sim 10^\circ\text{N}$ exceeds 0.2 m s^{-1} . The KC and MC are much stronger than the NEC, with velocity cores of $\sim 0.8 \text{ m s}^{-1}$. These two currents attach near the coast. Vertically, the major part of the NKM is trapped above the isopycnal surface of $\sigma_\theta = 26.8 \text{ kg m}^{-3}$. Below this isopycnal surface, the subsurface circulation is flowing in the direction opposite to the NKM circulation.

In this study, we defined two different domains: the NKM domain and the embedded WBC domain (Fig. 1). The sections bounded by 8°N , 130°E , and 18°N surround the NKM domain. The WBC domain encompassed the KC and MC in the meridional area bounded by 8°N to 18°N and from the coast to $\sim 250 \text{ km}$ offshore. The eastern boundary of the WBC domain runs almost parallel to the coastline of the Philippines. For the climatological mean, the NEC bifurcates at $\sim 14.9^\circ\text{N}$, distributing more water to the MC than to the KC. We used 14.9°N as the dividing line between the northern and southern sub-domains (Fig. 1). Separation of these sub-domains defined the physical features more clearly for our vorticity calculation and dynamic analyses.

According to Li and Gan (2022), the transports of KC at 18°N and MC at 8°N are composed of the transports determined by the effect of NEC intensity (INT), NEC migration (MIG), and NEC bifurcation location (BIF). The INT follows the variation of NEC intensity, which is large in spring/summer and small in late autumn. The contributions of MIG to

(14.9° to 18°N) and the southern (8° to 14.9°N) NKM sub-domains contribute the negative and positive vorticities, respectively.

Consistent with the seasonal meridional migration of the NEC and NB, negative vorticity from spring to summer and positive vorticity from autumn to winter dominate the NKM domain and WBC domain, respectively (Fig. 2). In each season, the strongest vorticity (either positive or negative) areas locate mainly in the WBC domain, which indicates that the strong velocity shear in the KC and MC contributes to most of the domain-integrated vorticity.

During spring and summer, the intensities of the NEC and the WBCs are strong, and the NEC is in its southernmost position. As a result, the negative relative vorticity in the NKM region occupies a large area with strong intensity, which reflects the anti-cyclonic circulation built by the intensified NEC-KC in spring (Fig. 2a). In autumn, the NEC weakens and moves north. Thus, the area of negative relative vorticity is squashed, and the NEC-KC weakens significantly. In spring and summer, the positive relative vorticity in the southern NKM sub-domain has a smaller area and higher intensity, while in autumn and winter, its area expands, and its intensity weakens. As a result, the cyclonic circulation of the NEC-MC system in the southern NKM sub-domain does not vary significantly with the seasons throughout the year.

According to Stokes' theorem, the intensity of the circulation along the boundary of the sub-domain interprets the domain-integrated vorticity:

$$-\underbrace{\iint_{\text{North NKM}} \nabla \times \mathbf{V} \, dA}_{\text{North NKM Vorticity}} = \underbrace{\int_{130^\circ\text{E}}^{\text{Coast}} \mathbf{V}s_{\text{NEC}} \, dS}_{\text{NEC Intensity at } 14.9^\circ\text{N}} + \underbrace{\int_{14.9^\circ\text{N}}^{18^\circ\text{N}} \mathbf{V}s_{\text{KC}} \, dS}_{\text{KC Intensity}} + \underbrace{\int_{\text{Coast}}^{130^\circ\text{E}} \mathbf{V}s_{18^\circ\text{N}} \, dS}_{\text{Intensity along NKM northern boundary}} + \underbrace{\int_{18^\circ\text{N}}^{14.9^\circ\text{N}} \mathbf{V}s_{130^\circ\text{E}} \, dS}_{\text{Intensity along NKM eastern boundary}} \quad (1)$$

$$\underbrace{\iint_{\text{South NKM}} \nabla \times \mathbf{V} \, dA}_{\text{South NKM Vorticity}} = \underbrace{\int_{130^\circ\text{E}}^{\text{Coast}} \mathbf{V}s_{\text{NEC}} \, dS}_{\text{NEC Intensity at } 14.9^\circ\text{N}} + \underbrace{\int_{14.9^\circ\text{N}}^{8^\circ\text{N}} \mathbf{V}s_{\text{MC}} \, dS}_{\text{MC Intensity}} + \underbrace{\int_{\text{Coast}}^{130^\circ\text{E}} \mathbf{V}s_{8^\circ\text{N}} \, dS}_{\text{Intensity along NKM southern boundary}} + \underbrace{\int_{8^\circ\text{N}}^{14.9^\circ\text{N}} \mathbf{V}s_{130^\circ\text{E}} \, dS}_{\text{Intensity along NKM eastern boundary}} \quad (2)$$

the KC and MC are opposite: the NEC migrates southward in early spring, weakening (strengthening) the KC (MC). The NEC migrates northward in late autumn, strengthening (weakening) the KC (MC). The contribution of BIF to WBCs, which reflects the transport across the 14.9°N section, is also out-of-phase for the KC and MC: the NEC bifurcation (NB) correlates with the NEC migration, moving southward in early spring which strengthens (weakens) the KC (MC), and the NB moves northward in late autumn which weakens (strengthens) the KC (MC). Because the effects of MIG and BIF almost compensate for each other, the INT or NEC intensity, dominates the KC and MC intensities.

To reveal the underlying dynamics of the Li and Gan (2022) study, we first project the KC and MC transports within the circulation in the northern and southern NKM sub-domains, respectively. Then we use the domain and layer-integrated vorticity equation to quantify the circulation and diagnose the associated coupled external and intrinsic dynamics for the KC and MC.

3.2. Spatiotemporal variability of the vorticity

To explore the underlying mechanism driving the variability in the WBCs, we linked the WBCs intensities with external vorticity fluxes entering/exiting the NKM sub-domains and with the vorticity arising from internal physical processes. In Fig. 2, we see that the seasonal variation of the relative vorticity in the entire NKM system has a domain that borders from 8°N to 18°N and from the coast to 130°E . The strong velocity shears in the northward KC and southward MC in the northern

where \mathbf{V} is the layer-integrated velocity. $\nabla \times \mathbf{V}$ is the relative vorticity. $\mathbf{V}s$ is the tangential velocity along the boundaries. The second terms on the right-hand sides of Equations (1) and (2) locates near the velocity cores of the KC and MC, representing the intensities of the KC and MC, respectively. In Equations (1) and (2), it is apparent that a fixed dividing line at latitude 14.9°N of the sub-domains is important and indispensable for isolating the clear physical controlling factors of the KC/MC intensity. We could only investigate the KC and MC independently, and quantify the contributions of the NEC intensity, migration, and bifurcation location to the KC/MC (Li and Gan, 2022) by using this fixed division. The fixed separation of the sub-domains was also necessary for the dynamic analyses that we present in the next section.

To indicate the links between WBC transport and the vorticity in the respective northern and southern sub-domains, we integrated the vorticity in each NKM sub-domain (Fig. 3a) and compared it with the respective KC and MC transports averaged from 14.9°N to 18°N and 8°N to 14.9°N , respectively. The correlation coefficient (CC) between the change rate of the northern domain-integrated relative vorticity and the averaged-transport in the KC reaches 0.82 (Fig. 3a), while the CC between the change rate of the southern domain-integrated relative vorticity and the averaged-transport in the MC is 0.78 (Fig. 3b). These high CCs indicate that the vorticities in both sub-domains reflect the intensities of the WBCs. In addition, the vorticities integrated in their respective WBC sub-domains correlate highly with the vorticities integrated in the corresponding NKM sub-domains and account for $\sim 95\%$ of the total vorticity in the NKM sub-domains (Fig. 3c and d), respectively.

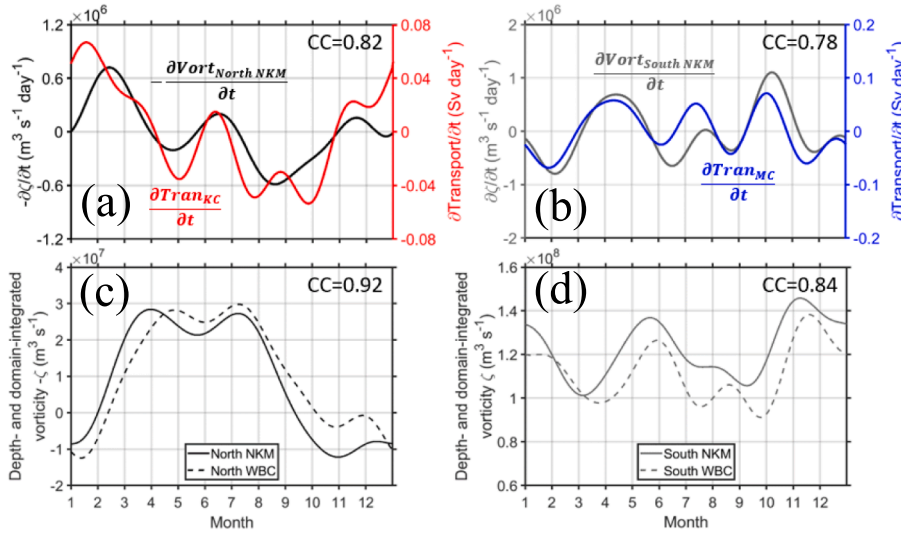


Fig. 3. Time series of the change rates of (a) the domain-integrated vorticity in the northern NKM sub-domain and along-stream-averaged KC transport, (b) the domain-integrated vorticity in the southern NKM sub-domain and along-stream-averaged MC transport. The time series of (c) the domain-integrated vorticity in the northern NKM sub-domain and northern WBC sub-domain, (d) the domain-integrated vorticity in the southern NKM sub-domain and south WBC sub-domain. The annual mean NB at latitude 14.9°N divides the NKM domain into the northern and southern sub-domains, and the NKM/WBC domains are shown in Fig. 1. Note that the change rate of the vorticity and domain-integrated vorticity in the northern sub-domain (left panel) have negative signs. CC denotes the correlation coefficient between the two variables in each figure.

The temporal variation of the domain-integrated vorticity in NKM and WBC sub-domains are similar, so we used the NKM sub-domains to further our analyses to dynamically connect the upstream NEC at the eastern boundary.

3.3. Coupling of external fluxes and intrinsic dynamics

Based on Stokes' theorem and the currents in the NKM sub-domains, the change of the domain-integrated relative vorticity connects to the variability in the WBCs. In this section, we use vorticity dynamics to investigate the interaction between external forcing (flux) and intrinsic dynamics that jointly control the vorticity variability in the NKM domain and, consequently, the variability of the WBCs.

To isolate the different physical processes, we adopted a domain- and layer-integrated vorticity equation (LIVE) within the NKM layer (from sea surface to the isopycnal surface of $\sigma_\theta = 26.8 \text{ kg m}^{-3}$). Following Gan et al. (2016), the LIVE is written as:

$$\overbrace{\Omega_{acc}}^{ACC} = \overbrace{\Omega_{cor}}^{NPV} + \overbrace{\Omega_{hadv}}^{NL} + \overbrace{\Omega_{hvisc}}^{HVISC} + \overbrace{\Omega_{vadv}}^{VADV} + \overbrace{\Omega_{pgf}}^{BPT} + \overbrace{\Omega_{vvisc}}^{NSC} \quad (3)$$

The complete form of equation (3) is described in Appendix A. By applying Stokes' theorem to Ω_{cor} , following Gan et al. (2016), we get:

$$\Omega_{cor} = \oint_S f V_n dS, \quad (4)$$

where S is the lateral boundaries of each NKM sub-domain. f is the planetary vorticity, and V_n is the inward velocity normal to the boundaries. As a result, Ω_{cor} physically indicates the net planetary vorticity, which is the residual part of the planetary vorticity influx and outflux in the NKM domain, which is closely linked to the volume transports of the NEC physical features (intensity, migration, and bifurcation location) described by Li and Gan (2022). The acceleration term (ACC) represents the change rate of the domain-integrated vorticity. The nonlinearity (NL) term indicates the nonlinear effect induced by relative vorticity convergence/divergence, which is strong within the WBC domain due to intensified boundary currents. The horizontal viscosity ($HVISC$) term is integrated in the domain to indicate the lateral friction along the domain boundary. The vertical advection ($VADV$) term represents the vertical relative vorticity flux. The bottom pressure torque (BPT) term indicates the curl of the horizontal component of the force normal to the bottom, which is exerted by the physical bottom on the fluid (Mertz and Wright 1992). The net stress curl (NSC) term is the sum of the surface and bottom stress curl. The surface stress

curl equals to the wind stress curl over the domain, and the bottom stress curl is proportional to the vertical shear of the horizontal velocity at the physical bottom of the NKM layer.

In the northern NKM sub-domain, the seasonal variation of the ACC (Fig. 4a) is highly correlated with the change rate of the vorticity integrated over the entire northern NKM domain, as shown in Fig. 3a. Thus, ACC reflects the strengthening or weakening of the circulation intensity in the NEC-KC system. We attribute the major source of the negative vorticity to NPV , which is mainly balanced by NL . Negative NPV means

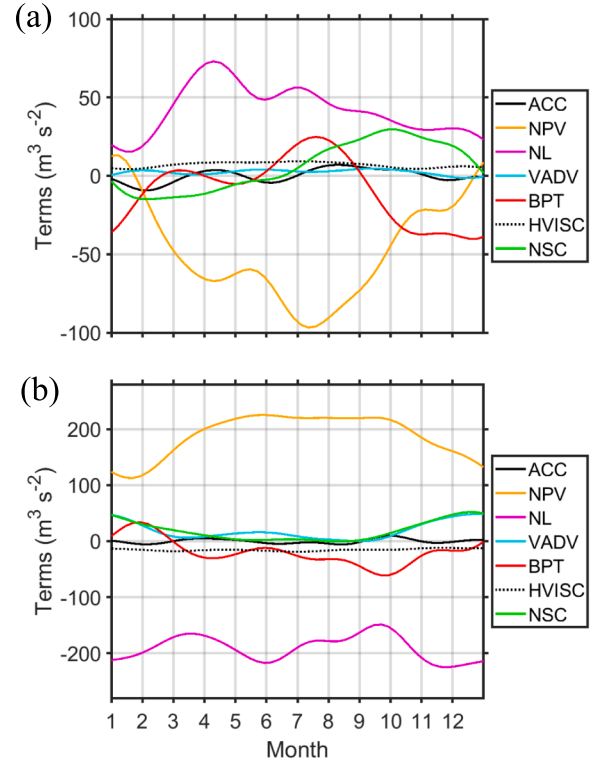


Fig. 4. Time series of the LIVE (Equation (5)) terms in (a) the northern and (b) the southern NKM sub-domains. ACC is the acceleration of the vorticity shown in the left-hand side of Equation (5). Positive and negative values of the right-hand side terms of Equation (5) indicate cyclonic and anti-cyclonic vorticity influx, respectively.

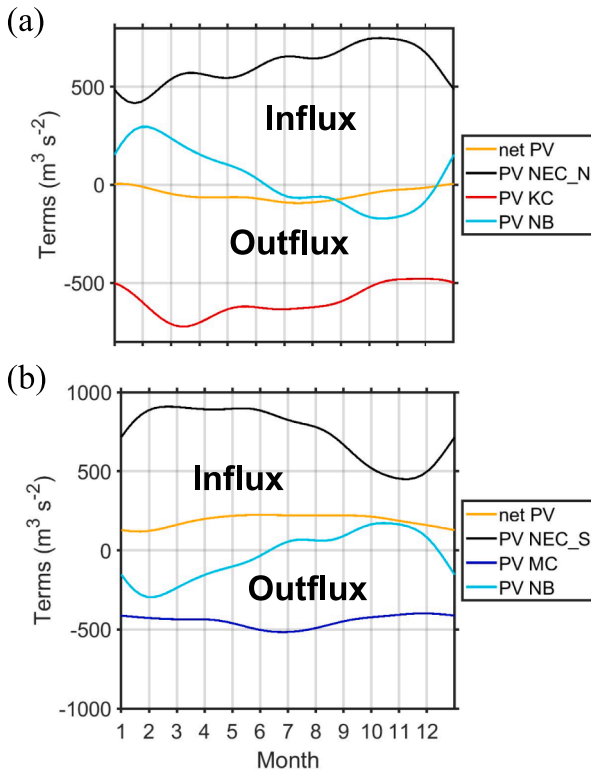


Fig. 5. Time series of the net planetary vorticity (NPV) in the (a) northern and (b) southern NKM sub-domains and the corresponding planetary vorticity fluxes across different sections: NEC_N, NEC_S, KC, MC, and NB. Positive values indicate a planetary vorticity influx and negative values indicate a planetary vorticity outflux.

there is a net loss of planetary vorticity in the domain because of the planetary vorticity outflux through the northern boundary of the northward flowing KC. The significant seasonality of the NPV term peaks in summer. After summer, the negative NPV and positive NL decreases, and the NSC induced by wind stress curl and BPT becomes significant. The combined effects of the bottom PGF and isopycnal tilting induce the BPT term and is related to the undercurrent system, which becomes energetic in late autumn (Li and Gan 2020). The VADV and HVISC terms have a limited effect on the vorticity balance for the sub-domain due to the weak vertical motion and small tangential velocity shear at the domain boundaries, respectively. The NSC term varies from negative in winter to positive in autumn, which indicates the role of the wind stress curl to the KC.

In the southern NKM sub-domain, the ACC, NPV, and NL terms vary weakly compared to the same terms for the northern sub-domain. The southern sub-domain NPV shows weaker seasonality than the northern sub-domain NPV because the small planetary vorticity (f) flux at low latitudes limits the variability of the total planetary vorticity fluxes in the sub-domain. Positive NPV indicates a net influx of planetary vorticity. Like in the northern NKM sub-domain, the NL term in the southern sub-domain offsets most of the NPV, and the other terms are small. The NSC is generally positive during the whole year and is strong in winter, which is consistent with the wind stress curl variation in the southern NKM sub-domain (Li and Gan 2022).

In summary, the intensity of the KC/MC, or integrated vorticity in the northern/southern NKM sub-domain, is externally dominated by the planetary vorticity carried by the NKM currents. The internal nonlinearity in the WBC domain mainly compensates for the planetary vorticity of the NKM currents, and the forcing at the surface (i.e., wind stress curl induced NSC) and at the bottom (i.e., BPT and VADV) of the NKM layer modulates the planetary vorticity seasonally.

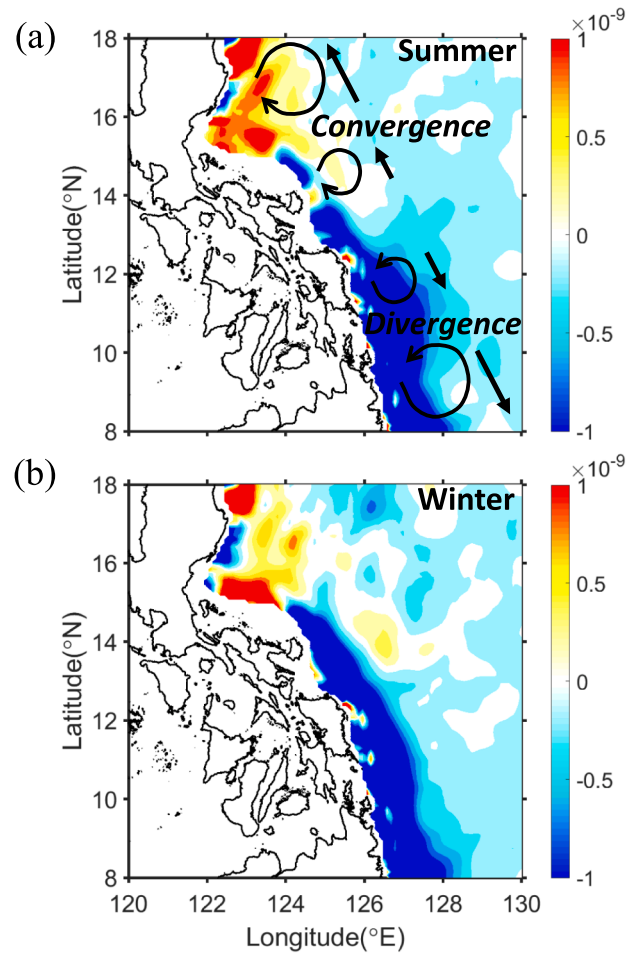


Fig. 6. Spatial pattern of the mean nonlinearity term (NL , $m s^{-2}$) in (a) summer and (b) winter.

3.3.1. Dominant external planetary vorticity flux

We interpreted the linked fluxes in the NKM system with their planetary vorticity budget. By applying Stokes' theorem, the NPV in the NKM domain consists of a planetary vorticity influx via the NEC and an outflux via the WBCs. Positive or negative NPV indicate that a certain amount of planetary vorticity remains in or is removed from each sub-domain, respectively. For those planetary vorticity fluxes contributed by the individual currents (i.e., PV NEC_N, PV NEC_S, PV KC, PV MC, and PV NB), the positive and negative values denote influges and outfluxes in each sub-domain, respectively (Fig. 5). The strengths of PV NEC_N and PV NEC_S are related to the NEC intensity and migration, which directly determine the volume transport of the NEC_N and NEC_S. Similarly, the PV NB is closely correlated with the NEC bifurcation location. Thus, the NEC physical modes described in Li and Gan (2022) dynamically link to the NPV discussed in this study, which is the dominant forcing of the NKM circulation.

In both sub-domains, the combined effects of an influx from the NEC (PV NEC_N, and PV NEC_S) and a planetary vorticity outflux across 14.9°N (PV NB) control the planetary vorticity outflux carried by the WBCs (i.e., PV KC, and PV MC) (Fig. 5). The planetary vorticity originating in the east (PV NEC_N and PV NEC_S) is the major source of the PV KC and PV MC. However, the PV NB compensates for the variability of the PV NEC_N (PV NEC_S) so that weak seasonality remains in the PV KC (PV MC). As a result, the intensities of the WBCs exhibit a seasonal variation like the seasonal variation that the PV KC and PV MC exhibit, peaking in spring and summer, respectively (Fig. 5).

The seasonal modes of the NEC characteristics including the intensity, migration, and bifurcation location discussed in Li and Gan (2022) are reflected clearly in the planetary vorticity budget. For the northern NKM sub-domain, PV_{NEC_N} peaks in autumn mainly because the NEC migrates northward (Fig. 5a). The meridional movement of NB induces the PV_{NB} influx (source) and outflux (sink) during winter and autumn, respectively, and is compensated for PV_{NEC_N} , in other words, by the effect of the NEC migration. From spring to summer, the large negative NPV in the northern sub-domain matches the stronger KC intensity that carries more planetary vorticity out of the northern sub-domain in the middle of the year. For the southern sub-domain, the PV_{NEC_S} peaks in spring due to the combined contributions of the strong intensity and southward migration of the NEC. In contrast to the seasonal variation of PV_{NB} in the north (Fig. 5a), PV_{NB} in the south (Fig. 5b) serves as a source (influx) of vorticity in autumn and a sink (outflux) in winter for the PV_{MC} . The positive NPV also peaks in the middle of the year, which suggests that the PV_{NB} influx with a larger planetary vorticity from the higher latitude (14.9°N) suppresses the PV_{MC} with smaller planetary vorticity at the lower latitude (8°N).

The planetary vorticity budget links closely with the NEC characteristics of the intensity, migration, and bifurcation location. The intensity of the KC/MC is highly correlated with the planetary vorticity outflux carried by the KC/MC, which is fueled by the planetary vorticity influx carried by the NEC_N and NEC_S . The effects of the NEC migration and bifurcation location to the WBCs are compensated, which is proven by the offset of PV_{NEC_N}/NEC_S and PV_{NB} . NPV showing a planetary vorticity loss (negative) and gain (positive) in the northern and southern sub-domains, respectively. The compensatory effects are caused by the latitude-dependent planetary vorticity difference in the currents (Fig. 5a). This NPV , as a residual vorticity, interacts with the intrinsic dynamics and jointly modulates the NKM circulation and WBC intensities.

3.3.2. Role of internal nonlinearity

Besides the dominant NPV , nonlinearity (NL) is the second important dynamic term determining the NKM circulation and WBCs (Fig. 4). Spatially, NL is significantly large in the WBC domain and attaches to the coast (Fig. 6) because the nonlinearity related to the strong velocity and velocity shear is prominent within the KC and MC. Based on Stokes' theorem, we interpreted the effects of NL term as the relative vorticity convergence.

$$\Omega_{adv} = -\nabla \bullet \zeta \quad (5)$$

where ζ is the relative vorticity, or velocity shear within the WBCs. Fig. 6 shows the spatiotemporal variability of the NL term for summer and winter. The difference between these two seasons is considerable, especially in the northern sub-domain (Fig. 4a), and the seasonal variation in the southern sub-domain is weak (Fig. 4b).

The nonlinearity in the WBCs is the main cause of the positive and negative NL in the northern and southern sub-domains, which compensate for a large portion of the NPV (Fig. 6). In the northern sub-domain, the KC, and its related negative relative vorticity, strengthens downstream (Fig. 2). In this case, the negative relative vorticity diverges within the KC, which leads to a net relative vorticity convergence (or positive NL ; Fig. 6a). In contrast, the downstream acceleration of the MC, and the associated intensification of the positive relative vorticity (Fig. 2), results in a net relative vorticity divergence (or negative NL) in the southern sub-domain (Fig. 6a).

Seasonally, the intensity and area of the positive NL in the northern sub-domain decrease from summer to winter (Fig. 6). As a result, the domain-integrated nonlinearity component is significantly seasonal (Fig. 4a). In the southern sub-domain, due to the variability of the NB location, the area of the negative NL enlarges in winter (Fig. 6b). However, the intensity of the negative NL decreases because of the weakening MC. These two effects compensate for each other and lead to a relatively stable domain-integrated NL in the southern sub-domain

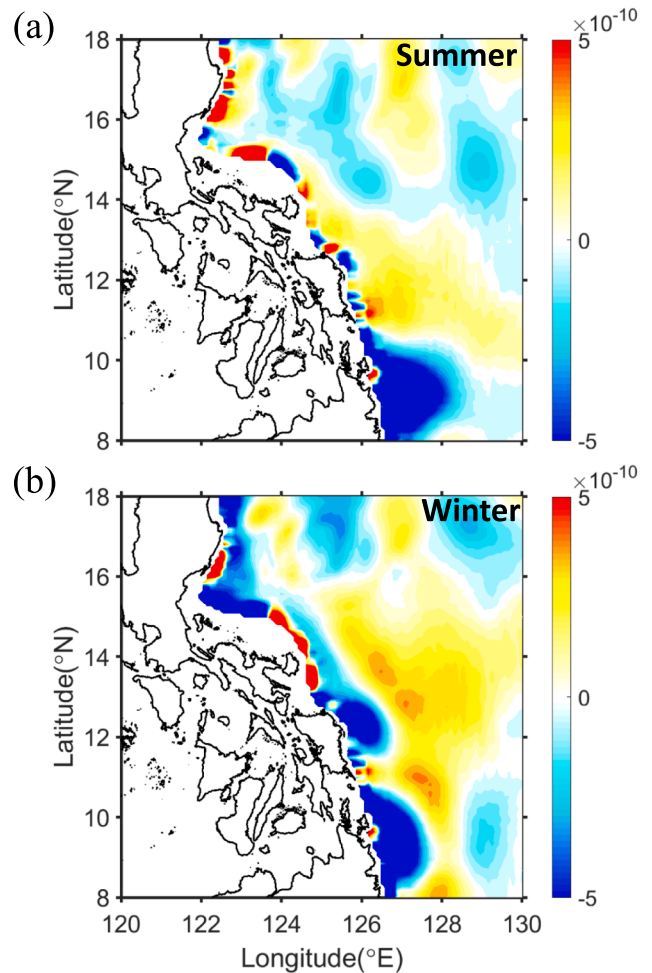


Fig. 7. Spatial pattern of the bottom pressure torque term (BPT , $m\ s^{-2}$) in (a) summer and (b) winter.

(Fig. 4b).

Nonlinearity, as the most important internal dynamic response of the NKM circulation, is prominent within the WBC domain due to the intensified velocity and velocity shear of the KC/MC. Convergence and divergence of the relative vorticity in the northern and southern sub-domains induce positive and negative NL to compensate for most of the externally forced NPV .

3.3.3. Effect of bottom pressure torque

BPT term represents the bottom PGF interacting nonlinearly with the tilting physical bottom of the NKM layer:

$$BPT = \frac{\partial H}{\partial y} \frac{\partial P}{\partial x} - \frac{\partial H}{\partial x} \frac{\partial P}{\partial y} \quad (6)$$

where H is the depth of the physical bottom. P is the pressure at the physical bottom of the NKM layer.

Physically, BPT is the curl of the horizontal component of the pressure at the bottom isopycnal surface. Obviously, the non-parallel isopycnal surfaces and isobars are necessary to generate BPT . BPT varies from positive in summer to negative in winter in the northern sub-domain and is stable in the southern sub-domain (Fig. 4). Therefore, we compared the patterns of BPT in summer and winter in Fig. 7.

Due to the complex PGF at the bottom isopycnal surface, BPT varies strongly in time (Fig. 4) and space (Fig. 7). In summer, the intensity of the BPT in the whole NKM domain is weak except for the region near the coast. During this time, the NKM circulation is not energetic, therefore

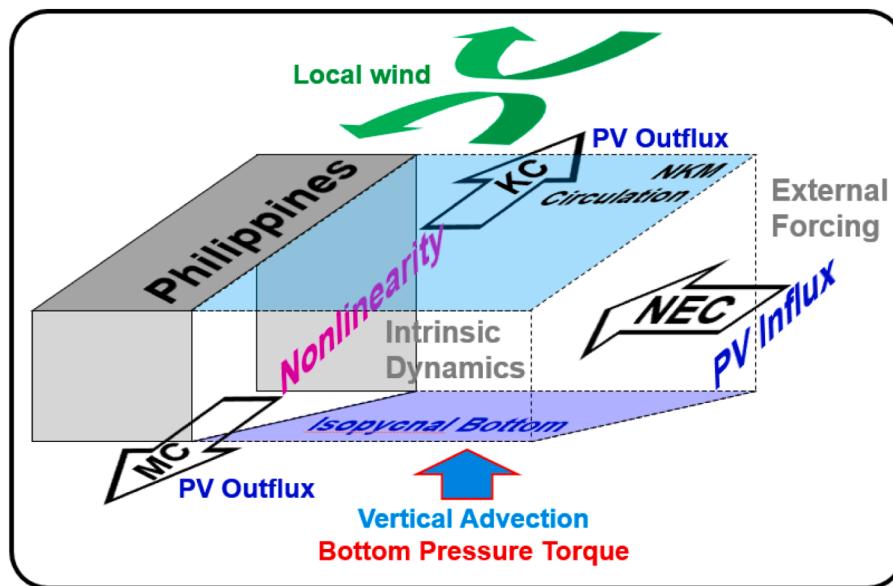


Fig. 8. Schematic of the external forcing and intrinsic dynamics controlling the KC, the MC, and the NKM circulation in the WPO.

the direction of the bottom PGF is almost parallel to the slope of the isopycnal surface. As a result, there is negligible *BPT* variability during spring and summer (Fig. 4). From December to February, the strength of the NKM circulation increases dramatically (Fig. 7) and the undercurrent circulation becomes energetic (Li and Gan 2020). The significant changes of the circulation in the upper layer and undercurrent system drive the non-parallel bottom PGF and the bottom slope, which induces stronger torque over the isopycnal surface. Thus, the intensity of *BPT*, positively or negatively, becomes more notable in winter (Fig. 7b).

In summary, we divided the WPO circulation into the northern and southern sub-domains so we could isolate the processes that control the KC and the MC in the NKM circulation system. Subsequently, based on Stokes' theorem, we used depth and layer-integrated vorticity equations to identify the dynamics for these processes. We found that *NPV* caused by the NEC characteristics of the intensity, migration, and bifurcation location externally dominate the KC/MC intensity, or circulation, in each sub-domain. The *NPV* provides the residual planetary vorticity of the fluxes carried in the NKM currents. *NPV* feeding vorticity into the circulation of both NKM sub-domains and further strengthening the WBCs, mostly compensated for the nonlinear processes within the WBCs. Meanwhile, wind stress curl imparts vorticity into the NKM circulation seasonally, and *BPT* at the bottom isopycnal surface influences the NKM circulation in winter. Our analysis demonstrates that the external forcing interacts with the intrinsic dynamics and jointly dominates the variability of the NKM circulation, and, therefore, the WBCs intensities.

4. Summary

Li and Gan (2022) conducted a kinematic investigation into the contributions of the NKM physical features: intensity, migration, and bifurcation location, to the WBCs' intensities. Based on their work, we studied the corresponding dynamics using simulations produced by a three-dimensional circulation model (CMOMS; <https://odmp.ust.hk/cmoms/>) (Gan et al. 2016a; Gan et al. 2016b).

We divided the NKM domain into the northern and southern sub-domains using the annual mean NB latitude at 14.9°N to define the separation. This division allowed us to independently investigate the physical processes within the KC and MC and isolate the two WBCs and their corresponding dynamics. The border between the northern and southern NKM sub-domains clearly defined the domain circulations and

the domain-integrated vorticity terms, which facilitated our dynamic analyses. Using Stokes' theorem, we found that the variabilities of the KC and MC correlate strongly with the circulation in the northern and southern NKM sub-domains, respectively, which links the intensities of the WBCs with the domain-integrated vorticity in the sub-domains.

We adopted the domain- and layer-integrated vorticity equation (LIVE) to isolate and quantify different physical processes and forcing mechanisms that control the NKM circulation. We found that the net planetary vorticity (*NPV*) dominates the intensity and variability of the circulation in both sub-domains (or, the intensity and variability of the WBCs), and the significant nonlinearity (*NL*) within the strong WBCs mostly compensates for the *NPV*. The planetary vorticity fluxes carried by the NKM currents determine *NPV*, and these fluxes represent the major external forcing related to the NEC physical features of the intensity, migration, and bifurcation location. Negative and positive *NPV* are in the northern and southern NKM sub-domains due to different planetary vorticity at the latitude of the NEC, in the KC, and in the MC. Strengthening of the NEC-KC/NEC-MC circulation drives the intensification of the intrinsic dynamic response of the nonlinearity within the WBC domain, due to the strong velocity and velocity shear in the boundary currents. Therefore, the effects of *NPV* and *NL* mostly offset each other throughout the year. The external planetary vorticity flux interacts with the intrinsic dynamics of the nonlinearity and dominates the circulation in each NKM sub-domain and the intensity of the KC/MC. Besides the dominant *NPV* and *NL*, the bottom pressure torque (*BPT*) associated with the isopycnal tilting due to the energetic undercurrent system in winter, and the surface stress curl induced by seasonal varying wind forcing, jointly modulate the seasonality of the NKM circulation and the WBC.

To conclude, we used Stokes' theorem to first link the WBC intensities with the NKM circulation and domain-integrated vorticity. Subsequently, we adopted vorticity dynamics to reveal that *NPV*, correlated with the NEC characteristics (intensity, migration, and bifurcation), dominates the NKM circulation and WBCs. The intrinsic dynamic response of *NL* induced by strong boundary currents compensates for most of the *NPV*, and the forcing at the NKM bottom (*BPT*) and sea surface (*NSC*) contribute vorticity to seasonally modulate the strengths of the WBCs. This study provides new insight on the forcing mechanisms of the NKM circulation and the variabilities of the WBCs (shown in Fig. 8), which are critical for our holistic understanding of water transport and underlying dynamics of the western tropical North Pacific.

Declaration of Competing Interest

The authors declare that they have no known competing financial interests or personal relationships that could have appeared to influence the work reported in this paper.

Data availability

Data will be made available on request.

Appendix A

Following Gan et al. (2016), we first layer-integrated the horizontal momentum equations in the NKM layer (from sea surface to the isopycnal surface of $\sigma_\theta = 26.8 \text{ kg m}^{-3}$), then take curl of the momentum equations to get the vorticity equation, and finally domain-integrated the vorticity terms in our focused NKM sub-domains. The domain- and layer-integrated vorticity equation (LIVE) is written as:

$$\begin{aligned} & \overbrace{\int_A \nabla \times \int_{Lb}^{Lu} \bar{V}_i dz dA}^{\Omega_{acc}} = - \overbrace{\int_A [(f\bar{u}D)_x + (f\bar{v}D)_y] dA}^{\Omega_{cor}} - \overbrace{\int_A \nabla \times \int_{Lb}^{Lu} (hadv) dz dA}^{\Omega_{adv}} + \overbrace{\int_A \nabla \times \int_{Lb}^{Lu} (hvisc) dz dA}^{\Omega_{hvisc}} \\ & + \overbrace{\int_A -\frac{1}{\rho_0} [J(Lb, P^{Lb}) + J(Lu, P^{Lu})] dA}^{\Omega_{pgf}} + \overbrace{\int_A \nabla \times \int_{Lb}^{Lu} (vadv) dz dA}^{\Omega_{adv}} + \overbrace{\int_A \nabla \times \int_{Lb}^{Lu} [K_v(\bar{V})_z] dz dA}^{\Omega_{hvisc}} \end{aligned} \quad (A1)$$

For the NKM layer, Lu is sea surface elevation, which is negligible as compared to the depth of Lb , the isopycnal surface of $\sigma_\theta = 26.8 \text{ kg m}^{-3}$. Thus, in our calculation, Lu is simplified as zero; $hadv$, $hvisc$, and $vadv$, are the horizontal advection, horizontal viscosity, and vertical advection terms in the momentum equations, respectively; f is the Coriolis parameter; and J is a Jacobean operator. The overbar refers to the layer average.

References

- Centurioni, L.R., Niiler, P.P., Lee, D.-K., 2004. Observations of inflow of Philippine Sea surface water into the South China Sea through the Luzon Strait. *J. Phys. Oceanogr.* 34, 113–121.
- Chen, C., Ruo, R., Paid, S., Liu, C., Wong, G., 1995. Exchange of water masses between the East China Sea and the Kuroshio off northeastern Taiwan. *Cont. Shelf Res.* 15, 19–39.
- Fairall, C., Bradley, E.F., Hare, J., Grachev, A., Edson, J., 2003. Bulk parameterization of air–sea fluxes: updates and verification for the COARE algorithm. *J. Clim.* 16, 571–591.
- Farris, A., Wimbush, M., 1996. Wind-induced kuroshio intrusion into the South China Sea. *J. Oceanogr.* 52, 771–784.
- Gan, J., Allen, J.S., 2005. On open boundary conditions for a limited-area coastal model off Oregon. Part I: Response to idealized wind forcing. *Ocean Model.* 8, 115–133.
- Gan, J., Liu, Z., Hui, C.R., 2016a. A three-layer alternating spinning circulation in the South China Sea. *J. Phys. Oceanogr.* 46, 2309–2315.
- Gan, J., Liu, Z., Liang, L., 2016b. Numerical modeling of intrinsically and extrinsically forced seasonal circulation in the China Seas: a kinematic study. *J. Geophys. Res. Oceans* 121, 4697–4715.
- Gordon, A.L., 1986. Inter-ocean exchange of thermocline water. *J. Geophys. Res. Oceans* 91, 5037–5046.
- Hu, D., M. Cui, 1989. The western boundary current in the far-western Pacific Ocean. In: *Proceedings of western international meeting and workshop on TOGA COARE, Inst. Fr. de Rech. Sci. pour le Deév. en Coop. Nouméa*, pp. 123–134.
- Hu, D., Cui, M., Qu, T., Li, Y., 1991. A subsurface northward current off Mindanao identified by dynamic calculation. In: *Elsevier Oceanography Series*. Elsevier, pp. 359–365.
- Hu, D., et al., 2013. Direct measurements of the Luzon Undercurrent. *J. Phys. Oceanogr.* 43, 1417–1425.
- Hu, D., et al., 2015. Pacific western boundary currents and their roles in climate. *Nature* 522, 299.
- Kashino, Y., Ishida, A., Kuroda, Y., 2005. Variability of the mindanao current: mooring observation results. *Geophys. Res. Lett.* 32.
- Kashino, Y., España, N., Syamsudin, F., Richards, K.J., Jensen, T., Dutrieux, P., Ishida, A., 2009. Observations of the North Equatorial current, Mindanao current, and Kuroshio current system during the 2006/07 El Niño and 2007/08 La Niña. *J. Oceanogr.* 65, 325–333.
- Li, J., Gan, J., 2020. On the formation dynamics of the North Equatorial Undercurrent. *J. Phys. Oceanogr.*
- Li, J., Gan, J., 2022. On the north equatorial current spatiotemporal modes and responses in the western boundary currents. *Prog. Oceanogr.*, 102820

Acknowledgements

The Key Research Project of the National Science Foundation of China (41930539) and the Hong Kong Research Grants Council (GRF 16206516) supported our research. CORE is the Center for Ocean Research in Hong Kong and Macau jointly established by QNLM and HKUST. We are also grateful for the support of The National Super-computing Center of Tianjin and Guangzhou. The Regional Ocean Modeling System (ROMS) produced the CMOMS data used in the paper, and these data are available from <https://odmp.ust.hk/cmoms/>.

- Liu, Z., Gan, J., 2012. Variability of the Kuroshio in the East China Sea derived from satellite altimetry data. *Deep Sea Res. Part I* 59, 25–36.
- Liu, Z., Gan, J., 2016. Open boundary conditions for tidally and subtidally forced circulation in a limited-area coastal model using the Regional Ocean Modeling System (ROMS). *J. Geophys. Res. Oceans* 121, 6184–6203.
- Liu, Z., Gan, J., 2017. Three-dimensional pathways of water masses in the South China Sea: a modeling study. *J. Geophys. Res. Oceans* 122, 6039–6054.
- Mellor, G.L., Yamada, T., 1982. Development of a turbulence closure model for geophysical fluid problems. *Rev. Geophys. Space Phys.* 20, 851–875.
- Mertz, G., Wright, D.G., 1992. Interpretations of the JEBAR term. *J. Phys. Oceanogr.* 22, 301–305.
- Nan, F., Xue, H., Yu, F., 2015. Kuroshio intrusion into the South China Sea: a review. *Prog. Oceanogr.* 137, 314–333.
- Nitani, H., 1972. On the deep and bottom waters in the Japan Sea. *Res. Hydrogr. Oceanogr.* 151–201.
- Qiu, B., Lukas, R., 1996. Seasonal and interannual variability of the North Equatorial Current, the Mindanao Current, and the Kuroshio along the Pacific western boundary. *J. Geophys. Res. Oceans* 101, 12315–12330.
- Qiu, B., Rudnick, D.L., Chen, S., Kashino, Y., 2013. Quasi-stationary north equatorial undercurrent jets across the tropical north Pacific Ocean. *Geophys. Res. Lett.* 40, 2183–2187.
- Qu et al., 1998. On the western boundary currents in the Philippine Sea. *J. Geophys. Res.: Oceans* 103, 7537–7548.
- Qu, T., Mitsudera, H., Yamagata, T., 1998a. On the western boundary currents in the Philippine Sea. *J. Geophys. Res. Oceans* 1978–2012 (103), 7537–7548.
- Qu, T., Chiang, T.L., Wu, C.R., Dutrieux, P., Hu, D., 2012. Mindanao Current/Undercurrent in an eddy-resolving GCM. *J. Geophys. Res. Oceans* 117.
- Ren, Q., Li, Y., Wang, F., Song, L., Liu, C., Zhai, F., 2018. Seasonality of the Mindanao current/undercurrent system. *J. Geophys. Res. Oceans* 123, 1105–1122.
- Sasaki, H., Nonaka, M., Masumoto, Y., Sasai, Y., Uehara, H., Sakuma, H., 2008. An eddy-resolving hindcast simulation of the quasiglobal ocean from 1950 to 2003 on the Earth Simulator. In: *High Resolution Numerical Modelling of the Atmosphere and Ocean*. Springer, pp. 157–185.
- Shepetchkin, A.F., McWilliams, J.C., 2005. The regional oceanic modeling system (ROMS): a split-explicit, free-surface, topography-following-coordinate oceanic model. *Ocean Model.* 9, 347–404.
- Tian, J., Yang, Q., Liang, X., Xie, L., Hu, D., Wang, F., Qu, T., 2006. Observation of Luzon strait transport. *Geophys. Res. Lett.* 33.
- Toole, J., Zou, E., Millard, R., 1988. On the circulation of the upper waters in the western equatorial Pacific Ocean. *Deep Sea Res. Part A. Oceanogr. Res. Papers* 35, 1451–1482.
- Wang, F., Zang, N., Li, Y., Hu, D., 2015. On the subsurface countercurrents in the Philippine Sea. *J. Geophys. Res. Oceans* 120, 131–144.